DISRUPTION OF KILOMETER-SIZED ASTEROIDS BY ENERGETIC COLLISIONS

E. Asphaug
SETI Institute / NASA Ames Research Center*
MS 245-3
Moffett Field, CA 94035, USA

S. J. Ostro
NASA Jet Propulsion Laboratory and California Institute of Technology
300-233
Pasadena, CA 91109-8099, USA

R. S. Hudson
School of Electrical Engineering and Computer Science
Washington State University
Pullman, WA 99164-2752, USA

D. J. Scheeres
Department of Aerospace Engineering and Engineering Mechanics
Iowa State University
Ames, IA 50011-3231, USA

W. Benz
Physikalisches Institut
University of Bern
Sidlerstrasse 5
CH-3012 Bern, Switzerland

*As of May 1 1998: Institute of Tectonics, Department of Earth Sciences, UCSC, Santa Cruz CA 95064

For submission to *Nature*

Direct all correspondence to: Dr. Erik Asphaug

NASA Ames Research Center MS 245-3

Moffett Field CA 94035 USA
voice: (650) 604-0786
fax: (650) 604-6779
email: asphaug@cosmic.arc.nasa.gov

Past collisions determine the current mechanical properties of asteroids, and hence their response to future collisions. To understand the evolution of their diverse shapes, structures and spin states, we model hypervelocity impacts into small asteroids using a modern 3D smooth-particle hydrocode (SPH3D) that takes material strength and fracture into account[1]. A radar-derived shape model[2] of the kilometer-sized near-Earth asteroid 4769 Castalia provides a template for the targets used in our simulations. Here we show collisional outcome to be extremely sensitive to the pre-existing configuration of fractures and voids, and that specific impactor velocity is more important than usually assumed. A porous asteroid (or one with deep regolith) damps the propagation of the shock wave, sheltering the most distant regions from disruption while greatly enhancing local energy deposition. Multi-component asteroids (*e.g.* contact binaries) are similarly preserved, because shock waves cannot effectively traverse their discontinuities. We find that the earliest impact sufficiently energetic to produce multi-component structure or deep regolith may strongly influence an asteroid's long-term evolution, and that an Earth-approaching object's internal structure may dramatically affect human efforts to alter its course.

Self-gravity, more than mechanical strength, determines the survival of asteroids larger than several hundred meters undergoing disruptive collisions. This result from numerical impact experiments[3] supports conjectures derived from images of minor planets[4] that gravitationally-bound aggregates of collisional debris (rubble piles) are common in our solar system. The near-Earth asteroid (NEA) population alone might include some 100,000 objects with sizes spanning this strength/gravity transition, where analytical scaling rules[5] for impact outcome fail. Detailed simulations are therefore required before we can adequately understand the impact evolution of NEAs and other small bodies, and before we can predict with confidence the outcome of a large-scale explosion in, on, or near a "doomsday rock" headed towards Earth.

Target shape matters greatly during impacts[6], so for the exploratory simulations presented here we adopt a representative asteroid instead of a sphere: specifically, a 3D shape model reconstructed[2] from radar images of NEA 4769 Castalia. This peanut-shaped

asteroid is 1.6 km in longest dimension, and is one of several Earth-crossing objects imaged in detail by radar[7]. Our three Castalia-shaped targets are made of (1) competent rock, (2) a pair of competent rocks separated by rubble, and (3) a 50% porous agglomeration of large boulders. These encompass several primary possible internal configurations of an asteroid. The material equation of state in each case is that of lunar gabbroic anorthosite[8], but substituting a specific density ρ=2.1 g cm^{-3} for the competent targets and 4.2 g cm^{-3} for the porous target, for a constant target mass 1.2×10^{15}g. Elastic moduli and flaw distribution parameters are derived from laboratory experiments in basalt[9]. (We do not suggest that NEAs are actually composed of basalt or anorthosite, but until adequate material descriptions become available for better analogs, we adopt this laboratory-verified "standard rock" for simulations.) Our code, SPH3D[1], models hypervelocity impacts into elastic solids with a plastic yield criterion, and models explicit fracture and dynamic fragmentation under principal tension. The numerical resolution of each target is ~130,000 particles. Unless otherwise noted, each target is struck by an 8 m radius, 5.8×10^{9} g basalt sphere (ρ=2.7 g cm^{-3}) at 5 km/s. This speed is typical of asteroid collisions[10] in the main belt, although for Earth-crossers a higher nominal impact speed may be appropriate. These impacts are equivalent in energy to the 17 kiloton Hiroshima bomb.

This impactor barely exceeds the disruption threshold for the non-porous intact target (Fig. 1). A ~500 m diameter damaged region forms, and distant fissures break the target into disconnected halves plus smaller pieces. We say that d*isruption* results when an intact asteroid is fragmented into pieces none more massive than half the original target, and that *dispersal* results when less than half the original target's mass remains gravitationally bound following the collision. Only ~10% of the target mass exceeds the nominal ~40 cm/s escape velocity, so this event is not dispersive. For an irregular, rapidly-rotating asteroid like Castalia (P=4 hrs), a detailed dynamical analysis is required to obtain the exact percentage. The impact imparts a Δv of ~7 cm/s to the non-escaping fraction's center of mass. Widespread surface fractures shown in Fig. 1 might become surface grooves such as those seen on the Martian satellite Phobos and on main-belt asteroids Gaspra and Ida[11]. The diameter of the fully damaged region is the same size as the crater diameter predicted by gravity scaling[12], *i.e.* if only gravity (and not strength)

were a factor, implying that intact, rocky ~1 km bodies are near the size transition between strength- and gravity-dominance for large scale cratering. Because strength has approximately equal influence here, ejecta velocities are greater than gravity scaling predicts, and ejecta deposited around this crater will be thin or absent.

The above simulation demonstrates that it is much easier to crack an intact target in two than to disperse it. This could be an important mechanism for producing contact-binary forms among asteroids. Our next exploration is therefore the effect of an identical impactor striking one lobe of an initially binary Castalia, with intact lobes separated by ~20 m of fully-damaged rubble (Fig. 2). Due to impedance mismatch, shock energy is reflected from the discontinuity back into the impacted lobe, which becomes utterly destroyed. The unimpacted lobe suffers only minor damage. Depending on *N*-body dynamics in the aftermath, the final outcome may be isotropic (a solid core mantled by the non-escaping fraction) or dichotomous. As before, approximately 10% of the target escapes; Δv is ~3 cm/s.

Porous targets are can be similarly resistant to disruption, because shock wave propagation is hindered by irregularities and voids, resulting in localized energy deposition. However, a target which is porous and also strengthless might be comparatively easy to disperse by impact or high-yield explosion. Figure 3 shows the aftermath of the same impactor striking the porous target, for comparison with Fig. 1; numerical resolution prevents us from separating the porous target into disconnected boulders, and hence the initial object is rigid. Almost all fracture damage (red) occurs within a ~500 m diameter hemisphere centered on the impact point, with only minor damage far from the impact. More important differences are revealed by Fig. 4, which shows cross-sections of particle velocity and internal energy 1.2 sec after projectile contact with the porous and non-porous targets. In the porous target, the shock dissipates rapidly with distance as PdV work is done in the collapse of pores, and as scattering prevents coherent departure of shock energy from the impact zone. The resultant increase in particle speed and internal energy extends to a distance where the shock wave dies out. By comparison, the shock in the non-porous target is broadcast with few hindrances to the farthest reaches of the asteroid, leading to some disruption at great distance, and to lower energy deposition (kinetic or thermal) near the impact. More than half the porous

target is accelerated beyond nominal escape velocity, and a *strengthless* rubble pile would be dispersed by this event, with a Δv of ~14 cm/s applied to the remaining $\sim 5 \times 10^{14}$ g body. In our moderately-fragmented *rigid* porous body, however, only the damaged region can escape, which it does: no ejecta returns to fill the excavated crater or to form an ejecta blanket. Since distal damage is hindered, a preponderance of large, pristine craters on an asteroid might imply a porous yet coupled interior, or else internal heterogeneity sufficiently great to scatter the shock and localize energy deposition.

The impact vapor and melt in our porous target penetrates the surface, rather than being directed immediately outward. This produces an ejecta pattern which is far from conical (compare the final trajectory vectors in Fig. 4); subsurface thermal alteration and material mixing is likely[13]. A more precise equation of state, and a thermal conductivity model, is required in our code before quantitative predictions can be made about the degree of alteration and mixing, but the effect seems significant. A large meteoroid hitting a fine-grained porous target is less likely to result in such efficient vapor interpenetration, although laboratory experiments[14] show that energy deposition remains highly localized in these cases as well.

We conclude by examining scale-equivalence in impacts. Many aspects of a collision might be invariant to velocity provided that a "coupling parameter" — essentially a hybrid between momentum (mv) and energy (mv^2) — is conserved[6]. Specifically, for solid rock targets, if $mv^{1.68}$ is held constant, the impact outcome should be the same. This relation has demonstrable merit in the case of hypervelocity cratering, at least in the gravity regime, provided the impact speed is always much faster than the target's sound speed. However, our simulations show that for impact speeds much lower than this (~5 km/s in our nonporous targets and ~4 km/s in our porous target), such invariances are poor descriptors of collisional outcome[15]. Fig. 5 compares the aftermath of a larger (20 m radius), slower (1 km/s) impactor, "equivalent" to the 8 m, 5 km/s impactor of Fig. 1. In each case the asteroid cracks in two, but the predominant fractures for the slower projectile radiate from the impact, instead of propagating parallel beneath the surface. The greater amount of intermediate damage (yellow) and the smaller crater bowl (red) imply that impact disruption and cratering in the outer solar system, where collision speeds are typically slower than ~1 km/s, might differ significantly from what current

modeling efforts[16] suppose. The expected equation-of-state differences among small bodies (ice versus rock, for instance) presents another dimension of study; having recently ported our code to parallel architectures[17], we are now ready to perform a broader, more detailed study.

The exploratory simulations presented here suggest that when a young, nonporous asteroid (if such exist) suffers extensive impact damage, the resulting fracture pattern largely defines the asteroid's response to future impacts. The stochastic nature of collisions implies that small asteroid interiors may be as diverse as their shapes and spin states. Detailed numerical simulations of impacts, using accurate shape models and rheologies, can shed light on how asteroid collisional response depends on internal configuration and shape, and hence on how planetesimals evolve. Detailed simulations are also required before one can predict the quantitative effects of nuclear explosions on Earth-crossing comets and asteroids, either for hazard mitigation[18] through disruption and deflection, or for resource exploitation[19]. Such predictions will require detailed reconnaissance concerning the composition and internal structure of the targeted object.

Acknowledgments: This research was conducted in part under the auspices of NASA's Planetary Geology and Geophysics Program. Part of this research was conducted at the Jet Propulsion Laboratory and the California Institute of Technology, under contract with the National Aeronautic and Space Administration (NASA).

FIGURE CAPTIONS

Figure 1. An initially intact rocky Castalia (1.6 km longest dimension) seen 0.3 seconds after impact by an 8 m radius basalt sphere at 5 km/s. The energy of this impact is equivalent to the Hiroshima explosion. Blue is intact rock; red is fully damaged rock, incapable of supporting tensile or shear stress. The shock wave has by this time crossed the target twice, and has dissipated below the fracture threshold of the target rock. Full hydrodynamic and dynamical evolution of the evolving crater bowl and the mobilized fragments will take hours. Thin slices through the target center are shown: blue ejected particles in the side view are pieces of the impactor, and will escape. The non-escaping fraction (~90%) of the asteroid is imparted a Δv of ~7 cm/s.

Figure 2. A contact-binary Castalia 0.3 seconds after impact by an 8 m radius basalt sphere striking at 5 km/s on one end. The red band about the waist is pre-damaged, underdense (1.7 g cm^{-3}) material which presents an impedance barrier for the shock, thereby reflecting its energy back into the impacted lobe. While damage to the impacted lobe is almost total, very little damage occurs in the distal lobe. The non-escaping fraction (~90%) of the asteroid is imparted a Δv of ~3 cm/s. Depending on where non-escaping ejecta finally settle, the final configuration may consist of an intact kernel surrounded by debris or a structurally-bifurcated object with bedrock on one side and rubble on the other.

Figure 3. A 50% porous Castalia 0.3 seconds after impact by an 8 m sphere at 5 km/s. The target is rigid, formed from connected spheres with sizes ranging from ~30 to ~100 m. (Numerical resolution prevents us from adding a plane of rubble between each sphere, in the manner of Fig. 2.) Top and side views are thin-sections, with black representing void space initially present in the porous configuration, not to be confused with impact disaggregation. Final fracture damage (red) is shown for comparison with Fig. 1, and is restricted to the region near the impact. More than half this target is accelerated beyond escape velocity, although only the fractured region can actually be mobilized. A true

rubble pile would be dispersed by this collision, with a ~14 cm/s Δv applied to the ~5 × 10^{14} g nonescaping fraction.

Figure 4. Comparison of particle speed (left, in log cm/s) and thermal energy (right, in log erg/g) for the porous (top) and nonporous (bottom) targets, at t=0.12 sec, seen in cross-section At this time in the simulation, the shock wave has progressed as a relatively coherent signal to the far surface of the nonporous target, carrying much of the impact energy away from the contact zone and creating the spallation fractures seen in Fig. 1. In the porous target, by contrast, the shock is scattered and its energy confined by the voids, resulting in a larger zone exceeding escape-velocity (red and yellow) but lower intermediate velocities (green) and lower levels of distal disruption (Fig. 3). The entire damaged zone in the porous target exceeds escape velocity, and none of the far surface exceeds a few mm/s. The result will be a crater without an ejecta blanket, and minor seismic degradation in the distal regions of the target. Arrows in the energy plot indicate particle velocity, and show the dramatic effect of projectile interpenetration on ejecta trajectory.

Figure 5. Comparison of fracture damage in the solid, non-porous Castalia for the original 8 m, 5 km/s projectile (top) versus a scale-equivalent 20 m 1 km/s projectile striking at the same point. While gross bulk aftermaths are the same (the target breaks in two, for instance), the surface-bounded spallation of the hypervelocity case (fractures propagating sub-parallel to the surface) is replaced by radial fissuring in the subsonic impact (fractures radiating from the impact point), and the crater diameter in the subsonic impact is considerably smaller. Twice as much (~25%) material escapes from the slower, larger impact, and the nonescaping fraction is accelerated by 7 cm/s.

REFERENCES

[1] Benz, W., and E. Asphaug, 1995. Simulations of brittle solids using smooth particle hydrodynamics. *Comp. Phys. Comm.*, **87**, 253-265.

[2] Hudson, R. S., and S. J. Ostro 1994. Shape of asteroid 4769 Castalia (1989 PB) from inversion of radar images. *Science* **263**, 940-943

[3] Asphaug, E. and H.J. Melosh 1993. The Stickney impact of Phobos: A dynamical model. *Icarus* **101**, 144--164. Asphaug, E. *et al.* 1996. Mechanical and geological effects of impact cratering on Ida. *Icarus* **120**, 158-184. Nolan, M.C., E. Asphaug, H.J. Melosh and R. Greenberg 1996. Impact craters on asteroids: Does strength or gravity control their size? *Icarus* **124**, 359-371. Love, S.J. and T.J. Ahrens 1996. Catastrophic impacts on gravity dominated asteroids. *Icarus* **124**, 141-155. Melosh, H.J. and E.V. Ryan 1997. Asteroids: Shattered but not dispersed. *Icarus* **129**, 562-564.

[4] Veverka, J. and P. Thomas 1979. Phobos and Deimos - A preview of what asteroids are like. In *Asteroids* (T. Gehrels, ed.), University of Arizona Press, Tucson, 628-651. Belton, M.J.S. *et al.* 1992. Galileo encounter with 951 Gaspra - First pictures of an asteroid. *Science* **257**,1647-1652. Belton, M.J.S. *et al.* 1996. Galileo's encounter with 243 Ida: An overview of the imaging experiment. *Icarus* **120**, 1-19. Veverka, J. *et al.* 1997. NEAR's flyby of 253 Mathilde: Images of a C asteroid. *Science* **278**, 2109-2112.

[5] Housen, K.R., R.M. Schmidt and K.A. Holsapple 1983. Crater ejecta scaling laws: Fundamental forms based on dimensional analysis. *J. Geophys. Res* **88**, 2485-2499. Holsapple, K.A. and R.M. Schmidt 1987. Point source solutions and coupling parameters in cratering mechanics. *J. Geophys. Res.* **92**, 6350-6376. Housen, K.R. and K.A. Holsapple 1990. On the fragmentation of asteroids and planetary satellites. *Icarus* **84**, 226-253.

[6] Asphaug, E. *et al.* 1996. Mechanical and geological effects of impact cratering on Ida. *Icarus* **120**, 158-184.

[7] Ostro, S.J. *et al.* 1991. Asteroid radar astrometry. *Astron. J.* **102**, 1490-1502.

[8] Ahrens, T.J. and J.D. O'Keefe 1977. Equations of state and impact-induced shock-wave attenuation on the moon. In *Impact and Explosion Cratering* (D.J. Roddy, R.O. Pepin and R.B. Merrill, eds.), Pergamon Press, NY, 639-656. Tillotson, J.H. 1962. Metallic equations of state for hypervelocity impact. *General Atomic Report* GA-3216.

[9] Nakamura, A. and A. Fujiwara 1991. Velocity distribution of fragments formed in a simulated collisional disruption. *Icarus* **92**, 132-146. Benz, W., and E. Asphaug 1995. Simulations of brittle solids using smooth particle hydrodynamics. *Comput. Phys. Comm.* **87**, 253-265.

[10] Bottke, W.F., M.C. Nolan, R. Greenberg and R.A. Kolvoord 1994. Velocity distributions among colliding asteroids. *Icarus* **107**, 255-268.

[11] Asphaug, E. and H.J. Melosh 1993. The Stickney impact of Phobos: A dynamical model. *Icarus* **101**, 144-164; Asphaug, E. *et al.* 1996. Mechanical and geological effects of impact cratering on Ida. *Icarus* **120**, 158-184.

[12] Housen, K.R., R.M. Schmidt and K.A. Holsapple 1983. Crater ejecta scaling laws: Fundamental forms based on dimensional analysis. *J. Geophys. Res* **88**, 2485-2499.

[13] Asphaug E. *et al.* 1997. Impact evolution of icy regoliths. *LPSC XXVIII Abstracts*, 63-64.

[14] Love, S.G., F. Hörz and D.E. Brownlee 1993. Target porosity effects in impact cratering and collisional disruption. *Icarus* **105**, 216-224.

[15] Fujiwara, A., P. Cerroni, D.R. Davis, E.V. Ryan and M. DiMartino 1989. Experiments and scaling laws for catastrophic collisions. In *Asteroids II* (R.P. Binzel, T. Gehrels and M.S. Matthews, eds.), University of Arizona Press, 240-265.

[16] Davis, D.R. and P. Farinella 1997. Collisional evolution of Edgeworth-Kuiper Belt objects. *Icarus* **125**, 50-60.

[17] Olson, K. M. and E. Asphaug 1998. A parallel smooth particle hydrodynamics code simulating solid materials with strength for the Cray T3E. In preparation.

[18] Ahrens, T.J. and A.W. Harris 1992. Deflection and fragmentation of near-Earth asteroids. *Nature* **360**, 429-433.

[19] *Resources of Near-Earth Space* (J.S. Lewis, M.S. Matthews and M.L. Guerrieri, eds.), University of Arizona Press, 1993.

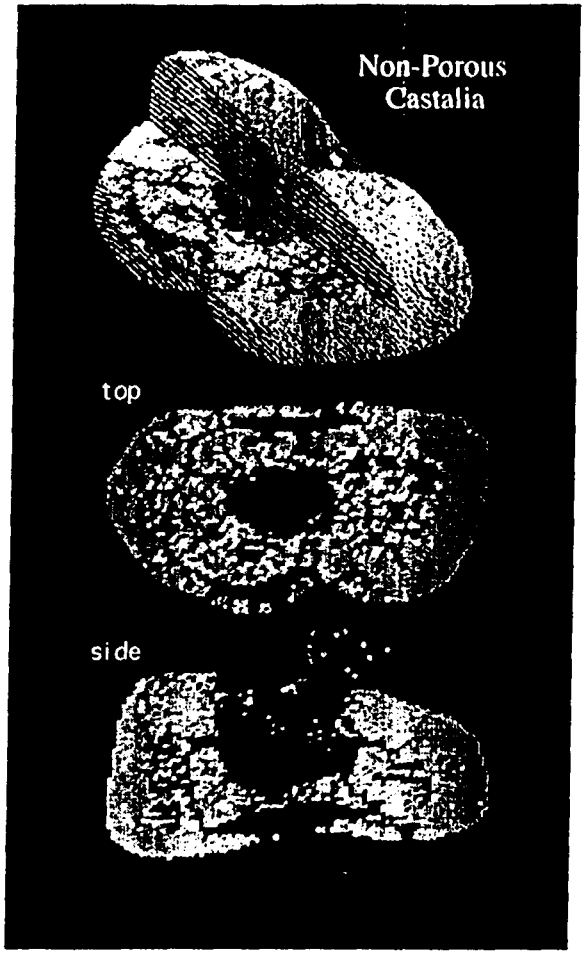

Figure 1. An initially intact rocky Castalia (1.6 km longest dimension) seen 0.3 seconds after impact by an 8 m radius basalt sphere at 5 km/s. The energy of this impact is equivalent to the Hiroshima explosion, although the mechanical efficiency of impacts is much greater. Blue is intact rock; red is fully damaged rock, incapable of supporting tensile or shear stress. The shock wave has by this time crossed the target twice, and has dissipated below the fracture threshold of the target rock. Full hydrodynamic and dynamical evolution of the evolving crater bowl and the mobilized fragments will take hours. Thin slices through the target center are shown; blue ejected particles in the side view are pieces of the impactor, and will escape. The non-escaping fraction (~90%) of the asteroid is imparted a delta-v of ~7 cm/s.

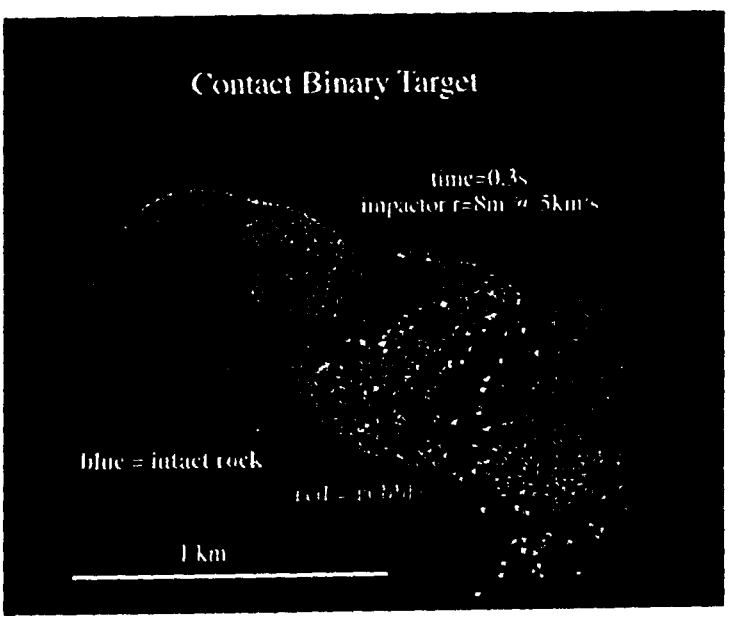

Figure 2. A contact-binary Castalia 0.3 seconds after impact by an 8 m radius basalt sphere striking at 5 km/s on one end. The red band about the waist is pre-damaged, underdense (1.7 g cm^-3) material which presents an impedance barrier for the shock, thereby reflecting its energy back into the impacted lobe. While damage to the impacted lobe is almost total, very little damage occurs in the distal lobe. The non-escaping fraction (~90%) of the asteroid is imparted a delta-v of ~3 cm/s. Depending on where non-escaping ejecta finally settle, the final configuration may consist of an intact kernel surrounded by debris or a structurally bifurcated object with bedrock on one side and rubble on the other.

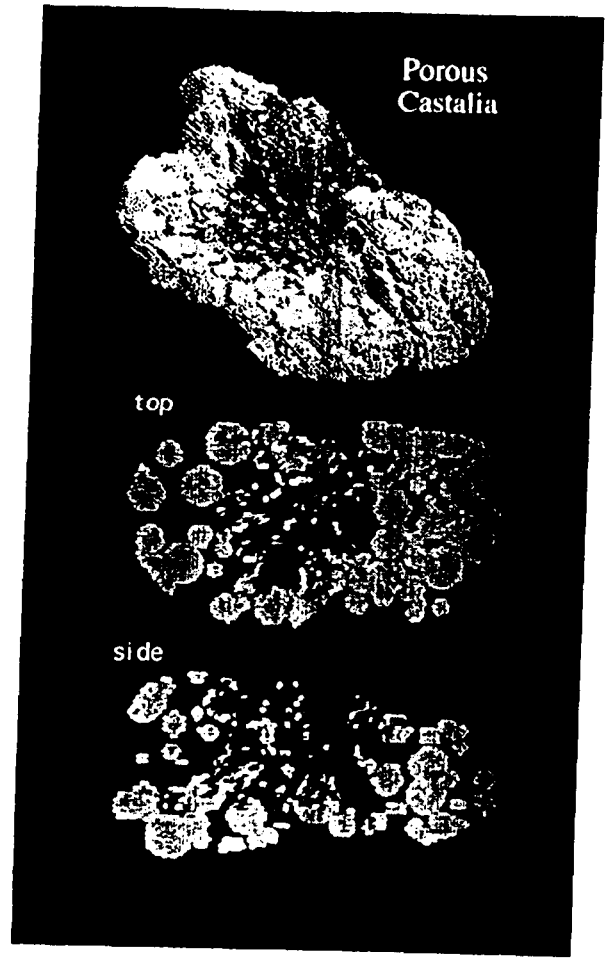

Figure 3. A 50% porous Castalia 0.3 seconds after impact by an 8 m sphere at 5 km/s. The target is rigid, formed from connected spheres with sizes ranging from ~30 to ~100 m. (Numerical resolution prevents us from adding a plane of rubble between each sphere, in the manner of Fig. 2.) Top and side views are thin-sections, with black representing void space initially present in the porous configuration, not to be confused with impact disaggregation. Final fracture damage (red) is shown for comparison with Fig. 1, and is restricted to the region near the impact. More than half this target is accelerated beyond escape velocity, although only the fractured region can actually be mobilized. A true rubble pile would be dispersed by this collision, with a ~14 cm/s delta-v applied to the ~5 x10^14 g nonescaping fraction.

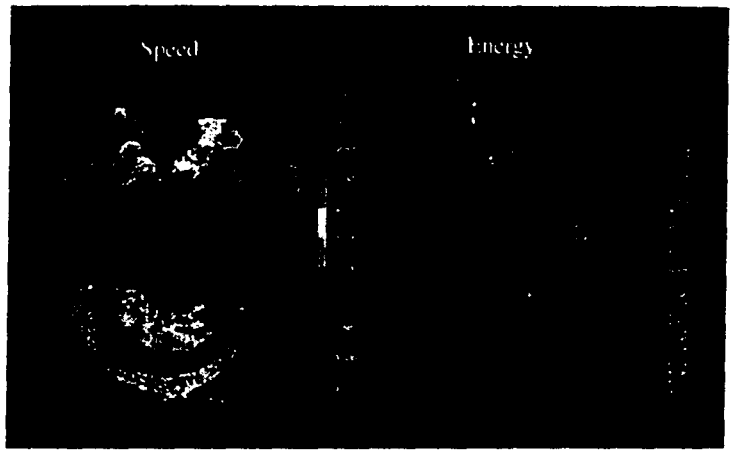

Figure 4. Comparison of particle speed (left, in log cm/s) and thermal energy (right, in log erg/g) for the porous (top) and nonporous (bottom) targets, at t=0.12 sec, seen in cross-section. At this time in the simulation, the shock wave has progressed as a relatively coherent signal to the far surface of the nonporous target, carrying much of the impact energy away from the contact zone and creating the spallation fractures seen in Fig. 1. In the porous target, by contrast, the shock is scattered and its energy confined by the voids, resulting in a larger zone exceeding escape velocity (red and yellow) but lower intermediate velocities (green) and lower levels of distal disruption (Fig. 3). The entire damaged zone in the porous target exceeds escape velocity, and none of the far surface exceeds a few mm/s. The result will be a crater without an ejecta blanket, and minor seismic degradation in the distal regions of the target. Arrows in the energy plot indicate particle velocity, and show the dramatic effect of projectile interpenetration on ejecta trajectory.

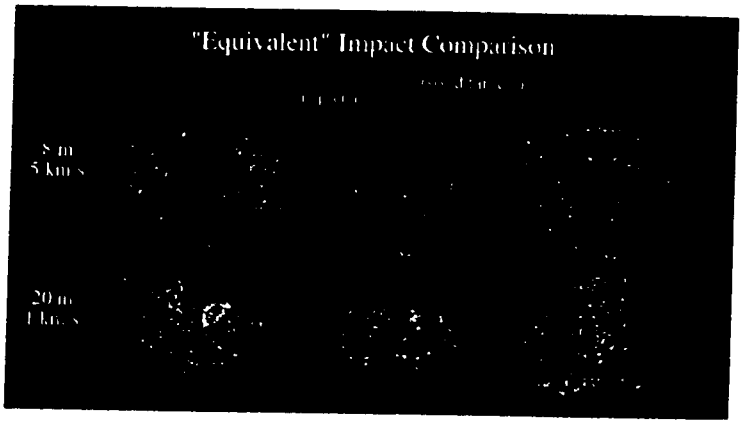

Figure 5. Comparison of fracture damage in the solid, non-porous Castalia for the original 8 m, 5 km/s projectile (top) versus a scale-equivalent 20 m 1 km/s projectile striking at the same point. While gross bulk aftermaths are the same (the target breaks in two, for instance), the surface-bounded spallation of the hypervelocity case (fractures propagating sub-parallel to the surface) is replaced by radial fissuring in the subsonic impact (fractures radiating from the impact point), and the crater diameter in the subsonic impact is considerably smaller. Twice as much (~25%) material escapes from the slower, larger impact, and the nonescaping fraction is accelerated by 7 cm/s.